Total reaction cross section for ^{12}C on ^{12}C, ^{40}Ca, ^{90}Zr, and ^{208}Pb between 10 and 35 MeV/nucleon

C. -C. Sahm,* T. Murakami,† J. G. Cramer, A. J. Lazzarini,‡ D. D. Leach, and D. R. Tieger§
Nuclear Physics Laboratory, University of Washington, Seattle, Washington 98195

R. A. Loveman**
Nuclear Physics Laboratory, University of Washington, Seattle, Washington 98195
and Nuclear Physics Laboratory, University of Colorado, Boulder, Colorado 80309

W. G. Lynch, M. B. Tsang, and J. Van der Plicht
National Superconducting Cyclotron Laboratory, Michigan State University, East Lansing, Michigan 48824
(Received 21 August 1986)

Elastic scattering angular distributions for ^{12}C on ^{12}C, ^{40}Ca, ^{90}Zr, and ^{208}Pb were measured for projectile energies between 10 and 35 MeV/nucleon. Total reaction cross sections were extracted by an optical model analysis and compared to the prediction of the Glauber model. This comparison suggests that the nucleus-nucleus total reaction cross section at intermediate and high energies is governed by the nucleon-nucleon cross section.

I. INTRODUCTION

At low energies the total reaction cross section (σ_R) for nucleus-nucleus scattering is determined primarily by the average collective nuclear behavior, and σ_R is essentially geometrical. As the collision energy is increased and characteristic wavelengths become shorter, one might expect the average nuclear behavior to become less important and the individual collisions of nucleons in the target with those in the projectile to constitute a larger part of the total reaction cross section. At the same time the total cross section for nucleon-nucleon scattering decreases dramatically with energy as the repulsive hard-core effects of the nucleon-nucleon interaction become dominant.

Using the approximation that the reaction cross section arises exclusively from the scattering of a single nucleon in the target on a single nucleon in the projectile (the optical limit of Glauber theory[1]), Alexander and Yekutieli[2] calculated σ_R at high energies ($E/A > 0.3$ MeV/nucleon) using measured nuclear charge distributions and experimental nucleon-nucleon cross sections. DeVries and Peng[3] included a simple Coulomb correction which allows one to apply the concept at intermediate energies. In this model, which we shall refer to as the "Glauber model," the rapid decrease of the nucleon-nucleon cross section between 10 and 300 MeV leads to a decrease in the nucleus-nucleus total reaction cross section, reaching a minimum at about 300 MeV/nucleon.

For $A > 4$ projectiles the carbon on carbon system stands out as the only system where extensive σ_R measurements have been made, in this case spanning 5–2100 MeV/nucleon. For other nucleus-nucleus systems the σ_R data are quite sparse. For carbon on heavier targets there are measurements at 83, 200, 250, and 300 MeV/nucleon. There are also measurements for ^{40}Ar on ^{60}Ni, ^{120}Sn, and ^{208}Pb at 44 MeV/nucleon.[4] In the present work we have measured total reaction cross sections for ^{12}C on ^{40}Ca, ^{90}Zr, and ^{208}Pb in the energy range between 10 and 35 MeV/nucleon. We also measured σ_R for the carbon on carbon system to check for consistency with earlier data. The method we have chosen for determining σ_R was first to measure forward-angle elastic scattering angular distributions, then fit these data with a model which generates an S matrix, and finally to calculate the σ_R from the S matrix thereby derived. For the carbon on carbon system a number of previous measurements have shown that this model-dependent technique gives results consistent with more direct measurements of σ_R.

II. EXPERIMENT

The experiments were performed using the S320 magnetic spectrometer of the National Superconducting Cyclotron Laboratory at Michigan State University. Self-supporting ^{12}C, ^{40}Ca, ^{90}Zr, and ^{208}Pb targets of about 1.0–1.5 mg/cm^2 thickness were used. The isotopic enrichment of the target material was better than 99%. These targets were bombarded with ^{12}C beams from the K500 superconducting cyclotron at energies of 120, 180, 300 and 420 MeV ($E/A = 10$, 15, 25, and 35 MeV/nucleon).

Interchangeable sets of aperture slits allowed setting the accepted solid angle of the spectrometer at between 0.0046 and 0.0626 msr. The spectrometer focal plane detector consisted of two single wire proportional counters separated by two ionization chambers, all in the same gas volume, and a thick plastic scintillator which stopped the particles. The position along the focal plane and hence the momentum of the incident particles was determined from the position along the wires, measured using charge division. The velocity of detected ions was determined by the time of flight using the cyclotron rf as a stop signal. The Z of an incident particle was obtained from the velocity and the energy loss in the two ionization chambers, the mass was determined from the velocity, and the momentum provided by the position measurement.

The spectrometer was set up with calculated field settings. These were changed slightly at the beginning of the run by optimizing position resolution. The corresponding energy resolution was typically $\cong 0.8$ MeV for the 420 MeV ^{12}C beam or 0.2%. This energy resolution was sufficient to separate elastic from inelastic events for all targets at all energies and angles. Relative scattering angles were known to an accuracy of 0.01°. The accuracy in determining absolute scattering angles was better than 0.05° and was limited principally by the measurement of 0° (the beam axis). This zero setting was found by two independent methods: (1) focusing the beam on the target and then rotating the spectrometer until the beam was centered on a removable scintillator at the focal plane, and (2) comparing the elastic scattering from one of the heavy targets at $-2°$ and at $+2°$.

Beam current, effective target thickness, and position of the beam on the target were monitored with a set of four plastic scintillators symmetrically mounted 0.159 m downstream from the target in the upper left, upper right, lower left, and lower right quadrants at angles of 6.4° with respect to the beam axis.

III. DATA ANALYSIS

A. Differential cross sections

Figure 1 shows a position spectrum of ^{12}C ions for the ^{12}C on ^{12}C reaction at 420 MeV. Both elastically scattered particles and those inelastically scattered from the 4.44 MeV first excited state are present. The full width at half maximum (FWHM) energy resolution of the elastic line is 0.8 MeV. Differential cross sections for elastic scattering were determined by normalizing the elastic line to the sum of the counts in the four monitor detectors. Because of the symmetric arrangement of the monitors, any errors in normalization arising from beam position variations will cancel in first order. For the lightest targets and the highest energies the monitor angle is well beyond the grazing angle, and so only a relative normalization can be obtained from the monitors. The absolute normalization was treated as a free parameter in fitting the data.

Figures 2–5 show measured elastic scattering angular distributions for the targets ^{12}C, ^{40}Ca, ^{90}Zr, and ^{208}Pb, respectively. The differential cross sections are divided by the relevant Mott or Rutherford Coulomb cross sections. The errors of the data are smaller than the symbol size and consist of the statistical errors and a contribution due to beam instabilities and the stability of the monitoring system, which was estimated to be 1.3%. The reproducibility of the data is illustrated in Fig. 2, where data taken in two different runs separated in time by about one year are shown as diamonds and circles.

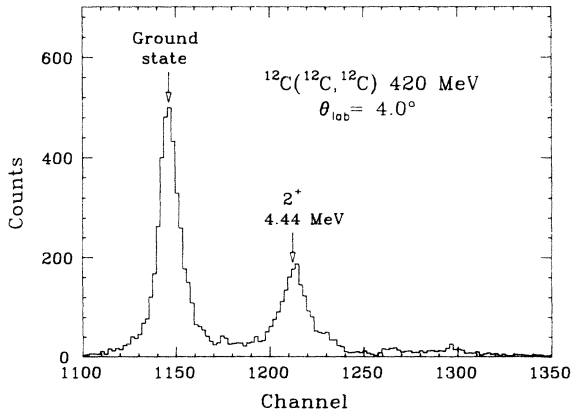

FIG. 1. Position spectrum for ^{12}C on ^{12}C taken at 180 MeV and 6° in the laboratory system.

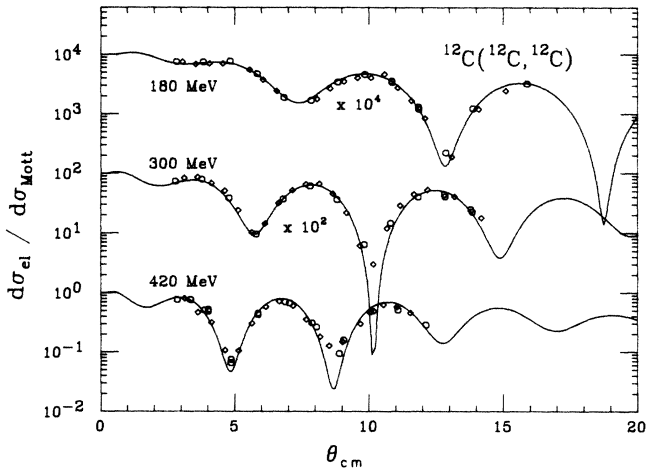

FIG. 2. Elastic scattering angular distributions for ^{12}C on ^{12}C. The circles indicate data taken in a run in 1984, and the diamonds indicate data taken in a 1985 run. The errors are smaller than the symbol size. The solid curves are the result of optical model fits with Woods-Saxon potentials for the real and the imaginary part.

B. Total reaction cross sections

The total reaction cross sections σ_R were determined by the optical model analysis described above. The angular distributions were fitted using the search version of the heavy ion optical model code HOP-2S. The total reaction

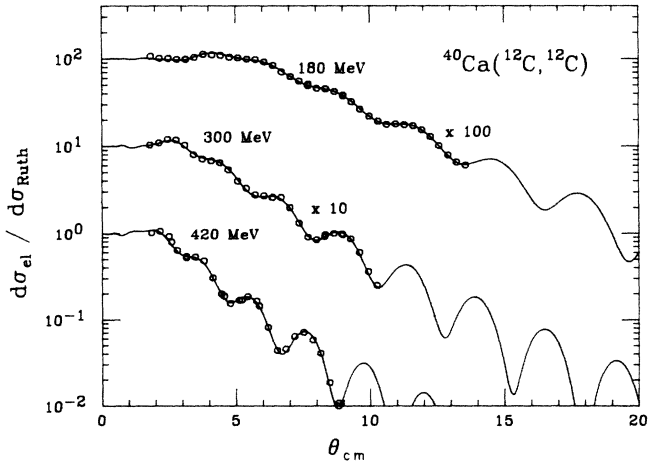

FIG. 3. Same as Fig. 2 for ^{12}C on ^{40}Ca.

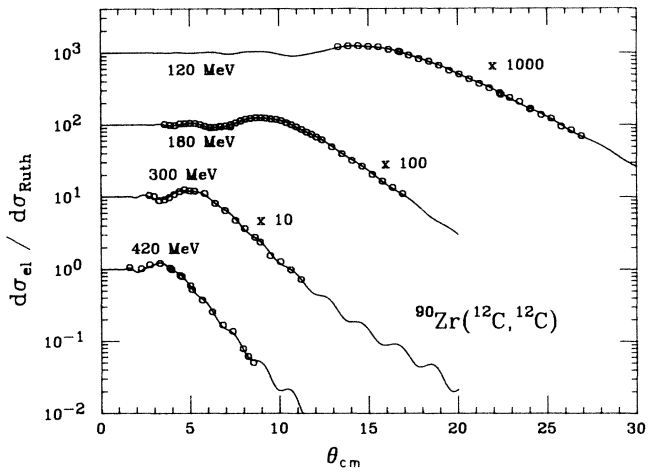

FIG. 4. Same as Fig. 2 for ^{12}C on ^{90}Zr.

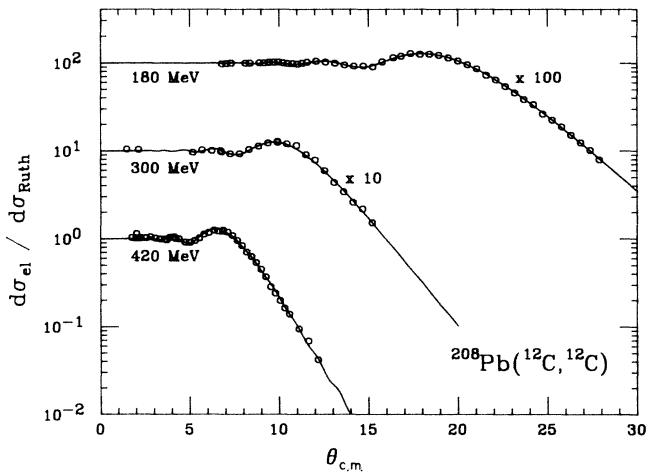

FIG. 5. Same as Fig. 2 for ^{12}C on ^{208}Pb.

cross section was calculated from the scattering matrix thereby obtained. These fits produced the lines drawn through the data points in Figs. 2–5. The angular distributions are reasonably well described using Woods-Saxon potentials for the real and imaginary parts of the optical potential. During the χ^2 minimization the central depth V of the real part was fixed. The absolute normalization of the data was allowed to vary. For the calculation of χ^2 the angle-averaging effect of the finite spectrometer angular aperture was taken into account. The optical potential parameters, χ^2 values, and total reaction cross sections are given in Table I.

In some cases the data did not adequately constrain the optical potential parameters. In particular, at 420 MeV and for the lead target at all energies an unphysically large real or imaginary diffuseness parameter was needed to minimize χ^2. In these cases the diffuseness parameters were fixed at values considered reasonable. Some examples demonstrating the sensitivity of σ_R to the choice of the diffuseness parameter are given in Table I. Parameters which were held fixed during the χ^2 minimization are indicated by an asterisk (*). With one exception the sensitivity of the total reaction cross section to the choice of diffuseness parameter was found to be small. Only in the case of the Zr target at 420 MeV was σ_R not well constrained. In this case the largest and smallest values of σ_R

TABLE I. Total reaction cross sections (σ_R) and parameters of Woods-Saxon optical potential. An asterisk (*) indicates that the parameter was held constant in search.

Target	E_{lab} (MeV)	V (MeV)	r_V (fm)	a_V (fm)	W (MeV)	r_W (fm)	a_W (fm)	χ^2	σ_R (mb)
^{12}C	180	250*	0.793	0.670	230.7	0.906	0.521	13.1	1331
^{12}C	300	250*	0.687	0.788	247.9	0.671	0.709	26.6	1296
^{12}C	420	250*	0.834	0.615	199.3	0.902	0.500*	107	1207
^{12}C	420	250*	0.818	0.627	220.5	0.844	0.550*	100	1219
^{12}C	420	250*	0.814	0.626	231.9	0.789	0.600*	94.9	1230
^{12}C	420	250*	0.803	0.636	425.0	0.654	0.650*	89.6	1243
^{12}C	420	250*	0.799	0.634	124.0	0.790	0.700*	86.0	1259
^{40}Ca	180	200*	0.966	0.624	226.2	0.831	0.798	1.65	2165
^{40}Ca	300	200*	0.801	0.837	276.9	0.897	0.653	2.58	2030
^{40}Ca	420	200*	0.657	1.054	273.0	0.884	0.658	9.03	1989
^{40}Ca	420	200*	0.870	0.75*	281.1	0.869	0.678*	31.0	2014
^{90}Zr	120	150*	1.017	0.689	217.9	0.953	0.672	1.04	2219
^{90}Zr	180	150*	0.880	0.874	174.4	0.979	0.618	0.95	2297
^{90}Zr	300	150*	0.809	0.999	191.4	1.020	0.546	2.96	2415
^{90}Zr	420	150*	0.934	0.781	207.7	0.890	0.834	2.70	2844
^{90}Zr	420	150*	0.795	1.041	256.7	0.967	0.600*	5.16	2512
^{90}Zr	420	150*	0.967	0.75*	250*	0.971	0.600*	8.85	2528
^{208}Pb	180	95*	1.059	0.78*	225*	1.023	0.643*	0.84	2873
^{208}Pb	300	95*	0.868	1.168	250*	0.985	0.662	1.86	3236
^{208}Pb	300	95*	1.034	0.80*	250*	1.006	0.656*	2.03	3333
^{208}Pb	420	95*	1.068	0.80*	200*	1.033	0.658	4.44	3561

were averaged and the error bar was assumed to be given by the two extreme values.

The method we have used here to obtain σ_R from the scattering data has the disadvantage of being somewhat model dependent. To investigate the extent of this model dependence we have also fitted the elastic data using a double-folded real optical potential of the type described in Ref. 5. Such potentials are generated by integrating the M3Y effective nucleon-nucleon interaction[6] over two Hartree-Fock nuclear matter densities.[7] We found that at the lower bombarding energies of 15 and 25 MeV/nucleon the folding model was fairly successful, giving fits that were typically slightly poorer in quality, with χ^2 values about twice that of Woods-Saxon fits but with σ_R values quite similar to those given in Table I.

However, it was found that at 35 MeV/nucleon the data for targets heavier than ^{12}C could not be adequately fitted with the folding model potentials. The best of these folding model fits are shown in Fig. 6. We speculate that the causes of this problem are the very deep and refractive central real potentials produced by folding and the reduced net absorption at higher energies. These effects combine to give strong "far-side" amplitudes describing flux deflected to negative angles by the strongly attractive folded potential. The enhanced far-side amplitudes of the folding model strongly interfere with the normal "near-side" amplitudes, leading to strong "two slit" interference oscillations in the angular distributions at backward angles. Interference oscillations of this strength are not present in the experimental data, as one can see in Fig. 6. We note, however, that in those cases where reasonable fits could be obtained with the folding model the resulting total reaction cross sections agreed to 5% with the results of the Woods-Saxon potential fits. We have therefore assigned a $\pm 5\%$ error to the total reaction cross section to account for the model dependence of the analysis procedure.

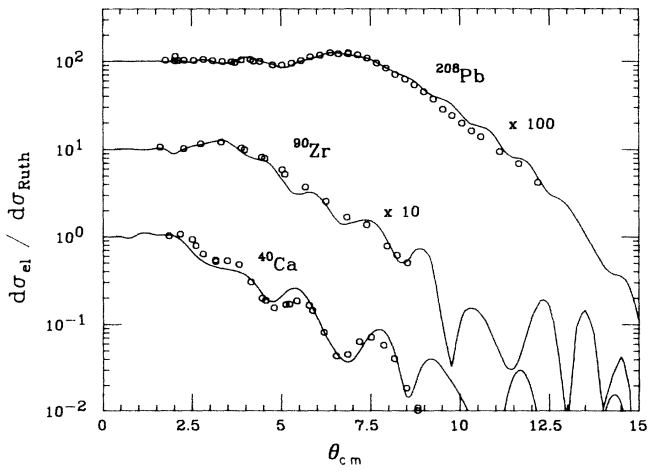

FIG. 6. Angular distributions for ^{12}C on ^{40}Ca, ^{90}Zr, and ^{208}Pb at $E/A = 35$ MeV/nucleon. The solid curves are best fits to the data using double-folded real optical potentials and Woods-Saxon imaginary potentials. The discrepancies between data and fit are taken as evidence for the inadequacy of the folding model at this energy.

IV. DISCUSSION

We first compare our results for the carbon on carbon system to data already available in the literature. Figure 7 shows as a function of the projectile energy per nucleon the total reaction cross section data derived from elastic scattering measurements,[8–12] from beam attenuation experiments,[13–16] and from an experiment which measured the sum of all reaction channels.[17] One can see that the data measured in this work agree very well with the systematics. In particular, the elastic scattering method yields results which are in agreement with the more direct measurements of the reaction cross section.

The solid curves in Fig. 7 are the result of a detailed microscopic Glauber model calculation by DiGiacomo and DeVries[18] using typical deep and shallow nuclear potentials. The deep-potential calculation reproduces the energy dependence of the measured reaction cross sections remarkably well, even at the lowest energies. The dashed curve in Fig. 7 shows the result of a much simpler Glauber calculation performed by the authors using the concepts outlined in Ref. 3. The simple Glauber calculation has no adjustable parameters and does not include three important effects: (1) Fermi motion which alters the velocities of colliding nucleons, (2) Pauli blocking which prevents n-n scattering to occupied momentum states, and (3) the strong nuclear force which deflects nuclear trajectories toward smaller collision distances. The agreement between the two calculations is apparently the result of a near cancellation between effects (1) and (2), which tend to decrease σ_R, and effect (3) which tends to increase σ_R. This cancellation of the Pauli and Fermi effects by the

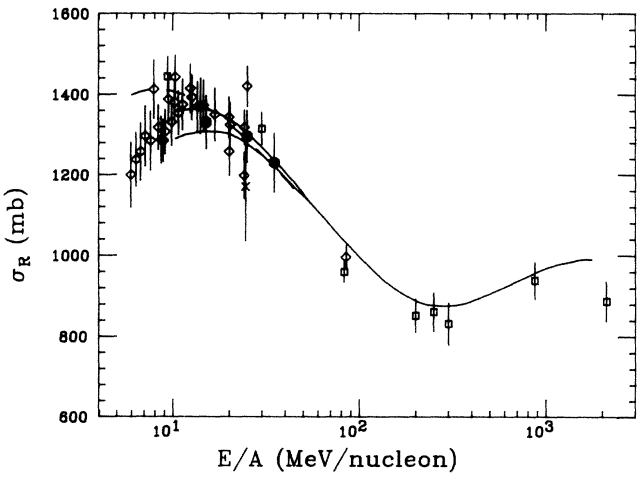

FIG. 7. Summary of total reaction cross section (σ_R) experimental data and calculations for the system ^{12}C + ^{12}C. The solid curves are the predictions of detailed microscopic Glauber model calculations of DiGiacomo and DeVries (Ref. 18) using deep (upper) and shallow (lower) nuclear potentials from the literature. The dashed curve is the prediction of a simple Glauber model calculation (Ref. 3) performed by the authors. The solid circles indicate present measurements, the open diamonds indicate other scattering measurements (Refs. 8–12), the open squares indicate transmission measurements (Refs. 13–16), and the single cross indicates a sum of directly measured reaction cross sections (Ref. 17).

nuclear potential is not well understood. It is perhaps a fortuitous accident, but there is also the possibility that it may have a more fundamental origin. A similar cancellation has been shown to occur in Glauber-model—based calculations[19] of nucleon-nucleus total reaction cross sections.

Figure 8 shows a summary of the total reaction cross section data for all targets investigated. We have also plotted the beam attenuation data taken at 83 MeV/nucleon by Kox *et al.*[15] These data are in qualitative agreement with earlier elastic scattering data[20] for the same systems. The solid curves shown in Fig. 8 are the predictions of the simple Glauber model discussed above. The dashed curves represent a "geometrical" strong absorption limit of σ_R and serve to illustrate the increase in transparency above 10 MeV/nucleon. It is clear from Fig. 8 that there is overall agreement between the data and the Glauber calculations for projectile energies to at least 35 MeV/nucleon. The Kox data at at 83 MeV/nucleon show poorer agreement with these Glauber predictions. We note that beam attenuation measurements with other targets at 200, 250, and 300 MeV/nucleon[16] support the validity of the simple Glauber model at higher energies. In particular, σ_R seems to reach a minimum at about 300 MeV/nucleon, which coincides with the minimum in the n-n total cross section.

The present data together with data available in the literature support the idea that the energy dependence of the nucleus-nucleus total reaction cross section is governed by the energy dependence of the nucleon-nucleon total cross section. However, it is not obvious why the simple Glauber calculation with the effects of Fermi motion, Pauli blocking, and the attractive nuclear force neglected is able to describe the energy dependence of σ_R for this variety of targets in the low energy region. Apparently, the cancellation of the effects of Fermi motion and Pauli blocking on one hand with the effect of nuclear attraction on the other, as described above, occurs for a wide variety of projectile-target combinations and energies.

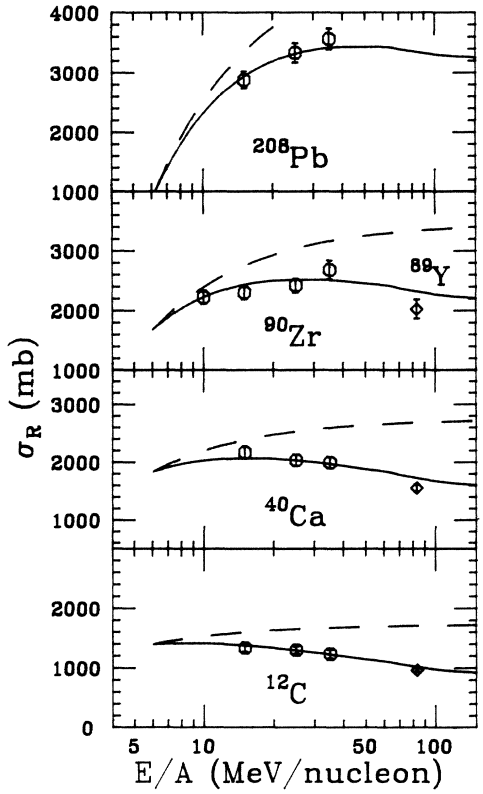

FIG. 8. Summary of total reaction cross section (σ_R) data and predictions for ^{12}C on mass 12, 40, 89, 90, and 208 targets. The solid curves are the predictions of the simple Glauber model calculation (Ref. 3) performed by the authors. The dashed curves represent a "geometrical" strong absorption limit of σ_R and serve to illustrate the increase in transparency above 10 MeV/nucleon. The three data points at 83 MeV/nucleon are taken from Ref. 15.

V. SUMMARY

We have measured angular distributions for elastic scattering of ^{12}C from ^{12}C, ^{40}Ca, ^{90}Zr, and ^{208}Pb between 10 and 35 MeV/nucleon. Reasonable fits of the angular distributions were obtained using Woods-Saxon optical potentials. The total reaction cross sections σ_R were calculated from the S matrix. The data for the carbon on carbon system agree within experimental uncertainties with the data from the literature. In particular, total reaction cross sections determined from elastic scattering agree with direct measurements of σ_R. These data are compared with the predictions of simple parameter-independent Glauber model calculations. The agreement between the data and the model suggests that the energy dependence of the nucleus-nucleus cross section at intermediate energies is governed by the energy dependence of the nucleon-nucleon cross section.

ACKNOWLEDGMENTS

We would like to thank G. Hinn for the fabrication of the targets and to thank the staff of the National Superconducting Cyclotron Laboratory for providing stable ^{12}C beams. This work was supported by the U.S. Department of Energy.

*Present address: Gesellschaft für Schwerionenforschung, GSI, Postfach 11 05 41, 6100 Darmstadt, Federal Republic of Germany.

†Present address: National Superconducting Cyclotron Laboratory, Michigan State University, East Lansing, MI 48824.

‡Present address: Kaman Instrumentation, 1500 Garden of the Gods Road, P.O. Box 7463, Colorado Springs, CO 80933.

§Present address: Laboratory for Nuclear Science, Massachusetts Institute of Technology, Cambridge, MA 02139.

**Present address: Nuclear Physics Laboratory, Box 446,

University of Colorado, Boulder, CO 80309.
[1]W. Czyz and L. C. Maximon, Ann. Phys. (N.Y.) **52**, 59 (1969).
[2]G. Alexander and G. Yekutieli, Nuovo Cimento **19**, 103 (1961).
[3]R. M. DeVries and J. C. Peng, Phys. Rev. C **22**, 1055 (1980).
[4]N. Alamanos, F. Auger, J. Barrette, B. Berthier, B. Fernandez, J. Gastenbois, L. Papineau, H. Doubre, and W. Mittig, Phys. Lett. **137B**, 37 (1984).
[5]G. R. Satchler and W. G. Love, Phys. Rep. **55**, 183 (1979).
[6]G. Bertsch, J. Borysowicz, H. McManus, and W. G. Love, Nucl. Phys. **A284**, 399 (1977).
[7]J. W. Negele, Phys. Rev. C **1**, 1260 (1970); *ibid.* **9**, 1054 (1974).
[8]A. J. Cole, W. D. M. Rae, M. E. Brandan, A. Dacal, B. G. Harvey, R. Legrain, M. J. Murphy, and R. G. Stokstad, Phys. Rev. Lett. **47**, 1705 (1981).
[9]M. Buenerd, P. Martin, R. Bertholet, C. Guet, M. Maurel, J. Mougey, H. Nifenecker, J. Pinston, P. Perrin, F. Schussler, J. Julien, J. P. Bondorf, L. Carlen, H. A. Gustafsson, B. Jakobsson, T. Johansson, P. Kristiansson, O. B. Nielsen, A. Oskarsson, I. Otterlund, H. Ryde, B. Schroder, and G. Tibell, Phys. Rev. C **26**, 1299 (1982).
[10]H. G. Bohlen, M. R. Clover, G. Ingold, H. Lettau, and W. von Oertzen, Z. Phys. A **308**, 121 (1982).
[11]M. Buenerd, A. Lounis, J. Chauvin, D. Lebrun, P. Martin, G. Duhamel, J. C. Gondrand, and P. de Saintignon, Nucl. Phys. **A424**, 313 (1984).
[12]H. G. Bohlen, X. S. Chen, J. G. Cramer, P. Fröbrich, B. Gebauer, H. Lettau, A. Miczaika, W. von Oertzen, R. Ulrich, and T. Wilpert, Z. Phys. A **322**, 241 (1985).
[13]J. Jaros, A. Wagner, L. Anderson, O. Chamberlain, R. Z. Fuzesy, J. Gallup, W. Gorn, L. Schroeder, S. Shannon, G. Shapiro, and H. Steiner, Phys. Rev. C **18**, 2273 (1978).
[14]C. Perrin, S. Kox, N. Longequeue, J. B. Viano, M. Buenerd, R. Cherkaoui, A. J. Cole, A. Gamp, J. Menet, and R. Ost, Phys. Rev. Lett. **49**, 1905 (1982).
[15]S. Kox, A. Gamp, R. Cherkaoui, A. J. Cole, N. Longequeue, J. Menet, C. Perrin, and J. B. Viano, Nucl. Phys. **A420**, 162 (1984).
[16]S. Kox, A. Gamp, C. Perrin, J. Arvieux, R. Bertholet, J. F. Bruandet, M. Buenerd, Y. El Masri, N. Longequeue, and F. Merchez, Phys. Lett. **159B**, 15 (1985).
[17]S. H. Simon, P. L. Gonthier, R. K. Choudhury, M. N. Namboodiri, K. Hagel, S. Kniffen, R. Patton, L. Adler, and J. B. Natowitz, Nucl. Phys. **A430**, 249 (1984).
[18]N. J. DiGiacomo and R. M. DeVries, Comments Nucl. Part. Phys. **12**, 111 (1984).
[19]N. J. DiGiacomo, R. M. DeVries, and J. C. Peng, Phys. Rev. Lett. **45**, 527 (1980).
[20]M. Buenerd, J. Pinston, A. J. Cole, C. Guet, D. Lebrun, J. M. Loiseaux, P. Martin, E. Monnand, J. Mougey, H. Nifenecker, R. Ost, P. Perrin, Ch. Ristori. P. de Saintignon, F. Schussler, L. Carlen, H. A. Gustafsson, B. Jakobsson, T. Johansson, G. Jönsson, J. Krumlinde, I. Otterlund, H. Ryde, B. Schroder, G. Tibell, J. B. Bondorf, and O. B. Nielsen, Phys. Lett. **102B**, 242 (1981).